Monograph:
Tokhi, O. and Leitch, R.R. (1991) The Robust Design of Active Noise Control Systems Based on Relative Stability Measures. Research Report. Acse Report 426 . Dept of Automatic Control and System Engineering. University of Sheffield

---

The robust design of active noise control systems based on relative stability measures

M O Tokhi * and R R Leitch **

* The University of Sheffield,
Department of Automatic Control and Systems Engineering,
PO Box 600,
Mappin Street,
Sheffield S1 4DU, U.K.

** Heriot-Watt University,
Department of Electrical and Electronic Engineering,
31-35 Grassmarket,
Edinburgh EH1 2HT, U.K.

Research Report No. 426

May 1991

Table of contents

Title	i
Table of contents	ii
Abstract	1
1. Introduction	1
2. Active noise control structure	6
3. Design of the controller	8
3.1. Practical limitations in controller design	9
4. System stability	17
4.1. The Nyquist stability criterion	18
4.1.1. Gain and phase margins	19
4.2. Required controller transfer function	20
4.2.1. Gain margin	22
4.4.2. Phase margin	30
5. Conclusion	35
6. References	36
Appendix A: The locus of constant distance ratio	39

Abstract

A design method for active noise control (ANC) systems operating in a three-dimensional non-dispersive propagation medium based on an analysis of the relative stability of the inherent feedback loop is presented. For practical systems the use of absolute stability is not useful; a system having an extremely long oscillatory response is unlikely to be accepted and would be liable to instability under small parameter variations. In this respect a measure of the relative stability can provide a more acceptable design criterion. This procedure results in a robust design able to operate under changing operating conditions, with guaranteed system stability under stationary and slowly varying conditions. The frequency domain stability conditions are interpreted as spatial conditions on the geometry of the ANC system. Practical limitations in the design of the controller owing to the geometric configuration of the system are also discussed.

1 Introduction

Active noise control uses the superposition of waves to achieve destructive interference and hence reduction of the sound level of an unwanted noise. This is realized by using detecting sensor(s) to obtain a signal that is coherent with the unwanted noise. The detected signal thus obtained is passed through a controller that has a suitable continuous transfer function. The output of the controller is used to drive a secondary source, the output of which is superimposed on the primary wave to achieve a destructive interference pattern and hence reduction in the primary noise level.

Active noise control was one of the earliest applications of electronics to the control of physical systems. Lueg filed for a patent in Germany in 1933 and in the USA in 1934 and was granted US Patent No. 2,043,416 in 1936 [1]. There has been considerable effort devoted to the theoretical and practical development of ANC systems since Lueg's first

controller [6, 7].

A feature of many noise sources is that they are not compact; noise is not emitted by one small part of the source but is distributed arbitrarily over the entire surface of the source. A distributed noise source is equivalent to a number of compact noise sources (multiple sources), distributed around the source surface, in which case the control problem is much more complicated than in the case of a single compact source. Here, a single detector and secondary source may not be sufficient to attenuate the unwanted noise but rather a number of them, depending on geometry limitations may be required.

The characteristics of many practical sources of noise are found to vary with operating conditions and hence time. For a time-varying source the performance of a controller with fixed frequency-dependent characteristics is no longer satisfactory. Here the system is required to be able to adapt to changes in the characteristics of the source. Moreover, as the required controller characteristics are found to be dependent on the system geometry, acoustic response of the medium and of transducers and other electronic equipment used, a change in any of these factors will reflect into the controller characteristics, hence requiring the controller characteristics to be updated. Through his experiments of reducing transformer noise Conover was the first to realize the need for a 'black box' controller that would adjust the canceling signal in accordance with information gathered at a remote distance from the transformer, as the performance of his ANC system was deteriorating from time to time due to the time-varying nature of the transformer noise [8]. Later it has been realized by numerous authors that it is an essential requirement for a practically successful ANC system to be adaptive [6, 9-18].

An acoustic wave traveling through a propagation medium is affected in amplitude as well as in phase due to the response characteristics of the medium, so that each component frequency of the noise emitted undergoes an amplitude and a phase change from

the point of emission to the point where it is detected. Moreover, acoustic feedback and reflected waves have a significant effect on the performance of an ANC system. These factors, together with the geometric arrangement of an ANC system, have a major effect on the stability of the system and can lead to practical limitations in the design of the controller.

It was realized rather early by both Jessel and Kido that the primary advantage of ANC systems is their ability to attenuate low-frequency noise [19-20]. This is an area of considerable interest because of the pervasiveness of low-frequency sources and the high cost, large bulk, and relative inefficiency of current passive hardware in low-frequency applications [5, 21]. Besides this, an advantage in the control of the one-dimensional propagation (duct noise) lies in the fact that active duct noise silencers produce no back-pressure.

Jessel, and others, also discovered some of the problems associated with reducing duct noise. Longitudinal duct modes leading to acoustic feedback, due to reflected waves, tend to confuse the controllers as to the exact level of the noise itself, since the detector microphone cannot distinguish between the noise and the reflected waves. This leads to system instability and/or no noise reduction in some frequency bands. To solve the longitudinal mode problem, so that the detector microphone detects the unwanted noise only, attempts have been made to use loudspeaker/microphone arrays. The acoustic tripole and acoustic dipole have been developed by Jessel and his co-workers and Swinbanks, respectively [19, 22]. They attempt to provide a canceling signal in the duct that propagates only in the downstream direction. The Chelsea System, developed by Leventhal, is formed by two secondary sources with the detector midway between them [4]. The controller is set to null the resultant of the secondary sources' waves at the detector location, thus isolating the detector from secondary source radiation. The performance of these systems shows

that they provide noise cancellation of up to 20-25 dB over a narrow band of less than an octave; the cancellation provided is optimum at only one frequency that is related to the physical spacing of secondary dipole sources [4, 23-24]. These systems have obvious geometry-related limitations. The control problem is also much more complex in such systems. Their third limitation is the so called 'tuning effect' due to the physical spacings of the microphone and loudspeakers relative to each other. By altering these spacings the system is tuned to a different centre frequency, with no significant improvement in the bandwidth of attenuation.

To achieve stable operation a design criterion based on relative stability measures of the system is introduced. In this manner, the design focuses on the derivation of a suitable transfer function for the controller so that it produces a mirror image of every detected frequency component of the noise. The dependence of controller characteristics on a number of frequency-dependent parameters within the system makes it possible to design and implement such a controller transfer function either in the continuous-time or discrete-time domain. Moreover, such a dependence provides an insight into the complexity of the controller and possibility of analyzing the system from the stability point of view so that stable operation of the system is ensured. Such a procedure results in a robust design of ANC systems.

The analysis focuses on ANC systems in stationary (steady-state) conditions. This corresponds to an ANC system with fixed controller of the required characteristics under situations where substantial variations in the characteristics of secondary source loudspeaker, transducers and other electronic equipment used do not occur. In an adaptive ANC system the controller adaptation mechanism is designed so that to result in the required controller characteristics. This means that once a steady-state (stationary) condition has reached the situation is equivalent to the case of the fixed controller. Therefore, in

an adaptive ANC system the analysis applies to periods where a steady-state condition has reached and substantial parameter variations do not occur. The stability and convergence of an adaptive controller in a time-varying (non-stationary/transient) non-linear environment is difficult to analyze and guarantee. However, the problem of instability under such a situation can be avoided by designing a suitable supervisory level control within the adaptive mechanism [18].

The controller design procedure is carried out in the continuous complex frequency, s, domain. At the implementation stage the controller transfer function is transformed to the discrete-time domain through an appropriate s to z transformation technique. Moreover, although the controller from this design procedure is obtained in the frequency-domain the actual implementation of the controller on a digital signal processor is performed in the time-domain [18]. Algorithms for implementing controllers in the frequency-domain have previously been considered by others [12].

2 Active noise control structure

A schematic diagram of the geometric arrangement of the general ANC structure known as the feedforward control structure (FFCS) is shown in Fig. 1a. The primary source emits an (unwanted) wave $p(t)$. A detector placed at a distance r_e relative to the primary source and a distance r_f relative to the secondary source detects this signal and transfers it to the controller C. After the detected signal has been adjusted in phase and amplitude it is emitted by the secondary source to be superimposed on the unwanted noise. The result of this superposition is observed at an observation point located at a distance r_g relative to the primary source and a distance r_h relative to the secondary source.

A block diagram of Fig. 1a is shown in the complex frequency s domain in Fig. 1b where

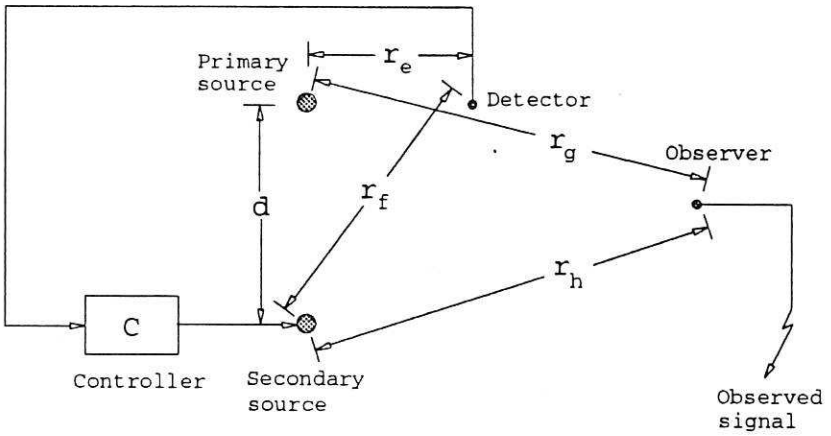

(a)

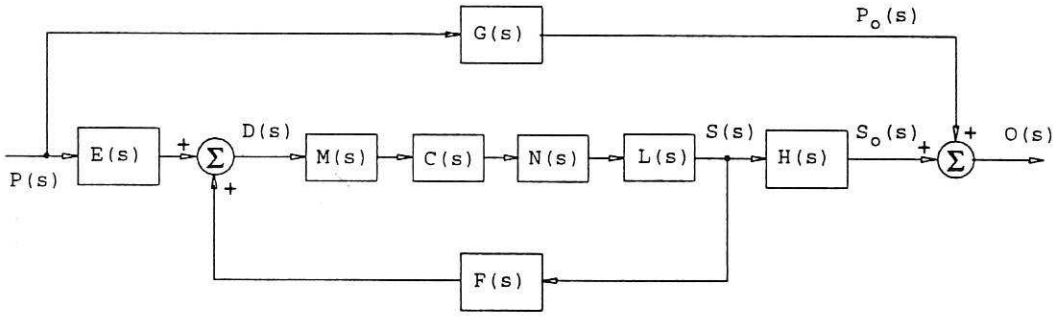

(b)

Fig. 1: Feedforward control structure;
(a) Schematic diagram,
(b) Block diagram.

$E(s)$ = transfer function of path r_e,

$F(s)$ = transfer function of path r_f,

$G(s)$ = transfer function of path r_g,

$H(s)$ = transfer function of path r_h,

$M(s)$ = transfer function of the detector,

$C(s)$ = transfer function of the controller,

$N(s)$ = transfer function of necessary electronics, and

$L(s)$ = transfer function of the secondary source.

It follows from this block diagram that the secondary path, i.e. through $C(s)$ to the observation point, attempts to compensate the primary path, i.e. through $G(s)$ to the observation point, such that the superposition of the primary and secondary waves results in cancellation at the observation point.

As seen in Fig. 1a the detector gives a combined measure of the primary and secondary waves that reach the detection point through the acoustic paths r_e and r_f respectively. The secondary wave thus reaching the detector forms a closed feedback loop (Fig. 1b) that can cause the system to become unstable. Therefore, a careful consideration of this loop is necessary in the design stage.

3 Design of the controller

The controller in an ANC system requires a careful consideration in the design stage. A controller intended for application in an ANC system should be capable of properly adjusting the amplitude and phase of every frequency component of a detected primary wave. Moreover, as noted in Fig. 1, due to acoustic feedback from the secondary source to the detector, stability conditions must be considered so that good system performance is

ensured.

The objective with the structure in Fig. 1 is to reduce the observed signal to zero. This requires that the observed primary and secondary signals should be equal in amplitude and opposite in phase;

$$P_o(s) = -S_o(s) \tag{1}$$

Obtaining the primary and secondary signals $P_o(s)$ and $S_o(s)$ from Fig. 1b, substituting into equation (1) and solving for $C(s)$ yields

$$C(s) = \frac{G(s)}{M(s)N(s)L(s)\Delta(s)} \tag{2}$$

where

$$\Delta(s) = F(s)G(s) - E(s)H(s) \tag{3}$$

Equation (2) represents the required controller transfer function for optimum cancellation of the unwanted noise over the frequency range of interest.

3.1 *Practical limitations in controller design*

It follows from equation (2) that for a particular detector and secondary source with necessary electronic components, the controller characteristics required for optimum cancellation at an observation point are dependent on the characteristics of the acoustic paths from the primary and secondary sources to the detector and observer locations. Any combination of the detector and observer locations with respect to the primary and secondary sources requires a particular controller characteristic. The effect of change in the location of the detector and/or observer, with respect to the primary and secondary sources must be considered. In particular, if the detector and observer are located such that $\Delta(s)$ in equation (2) becomes zero then the critical situation of an infinite-gain controller requirement arises.

The locus of such points in the medium (as a practical limitation in the design of the controller) is therefore of crucial interest.

Let the the detector and observer be located so as to result in $\Delta(s) = 0$. Under such a situation equation (2) for periodic waves ($s = j\omega$) yields

$$\frac{F(j\omega)}{E(j\omega)} = \frac{H(j\omega)}{G(j\omega)} \tag{4}$$

$E(j\omega)$, $F(j\omega)$, $G(j\omega)$ and $H(j\omega)$ are the frequency responses of the acoustic paths through the distances r_e, r_f, r_g and r_h, respectively; thus

$$\begin{aligned} E(j\omega) &= \frac{A}{r_e}\, e^{-j\frac{2\pi}{\lambda} r_e} \quad ; \quad F(j\omega) = \frac{A}{r_f}\, e^{-j\frac{2\pi}{\lambda} r_f} \\ G(j\omega) &= \frac{A}{r_g}\, e^{-j\frac{2\pi}{\lambda} r_g} \quad ; \quad H(j\omega) = \frac{A}{r_h}\, e^{-j\frac{2\pi}{\lambda} r_h} \end{aligned} \tag{5}$$

where λ is the signal wavelength and A is a constant.

Substituting for $E(j\omega)$, $F(j\omega)$, $G(j\omega)$ and $H(j\omega)$ from equation (5) into equation (4) and simplifying yields

$$\left(\frac{r_e}{r_f}\right) e^{-j(r_f - r_e)\frac{2\pi}{\lambda}} = \left(\frac{r_g}{r_h}\right) e^{-j(r_h - r_g)\frac{2\pi}{\lambda}}$$

This equation is true if and only if the amplitudes as well as the exponents (phases) on either side of the equation are equal. Thus,

$$\begin{aligned} \frac{r_e}{r_f} &= \frac{r_g}{r_h} = a \\ r_f - r_e &= r_h - r_g \end{aligned} \tag{6}$$

Equation (6) define the locus of points for which $\Delta(j\omega) = 0$ and the controller is required to have an infinitely large gain for optimum cancellation to be achieved at the observation point. Note that these equations are in terms of the distances r_e, r_f, r_g and r_h

only. Therefore, the critical situation of $\Delta(j\omega) = 0$ in a non-dispersive three-dimensional propagation medium is determined only by the detector and observer locations relative to the primary and secondary sources. Two possible cases, $a = 1$ and $a \neq 1$, are considered.

Unity distance ratio

This is equivalent to placing the microphone on the centre node of the dipole. In such a situation equation (6) yields

$$\frac{r_e}{r_f} = 1 \quad \text{and} \quad \frac{r_g}{r_h} = 1 \tag{7}$$

If the locations of the primary and secondary sources, in the three-dimensional propagation medium are fixed, then each relation in equation (7) defines a surface plane perpendicularly bisecting the line joining the primary and secondary source locations (see Appendix A). This plane for the primary and secondary sources located at points (0, 0, 0) and (u_s, v_s, w_s), respectively, with a distance d apart in a three-dimensional *UVW*–space, shown in Fig. 2, is described by

$$\frac{u}{(\frac{d^2}{2u_s})} + \frac{v}{(\frac{d^2}{2v_s})} + \frac{w}{(\frac{d^2}{2w_s})} = 1$$

which intersects the *U*–, *V*–, and *W*–axes at the points $(\frac{d^2}{2u_s}, 0, 0)$, $(0, \frac{d^2}{2v_s}, 0)$, and $(0, 0, \frac{d^2}{2w_s})$ respectively. This plane is shown in Fig. 3. If the detector is placed at any point on this plane and if at the same time the observer location coincides with a point on this plane then the 'critical situation' of $\Delta(j\omega) = 0$ occurs and the controller is required to have an infinitely large gain for optimum cancellation.

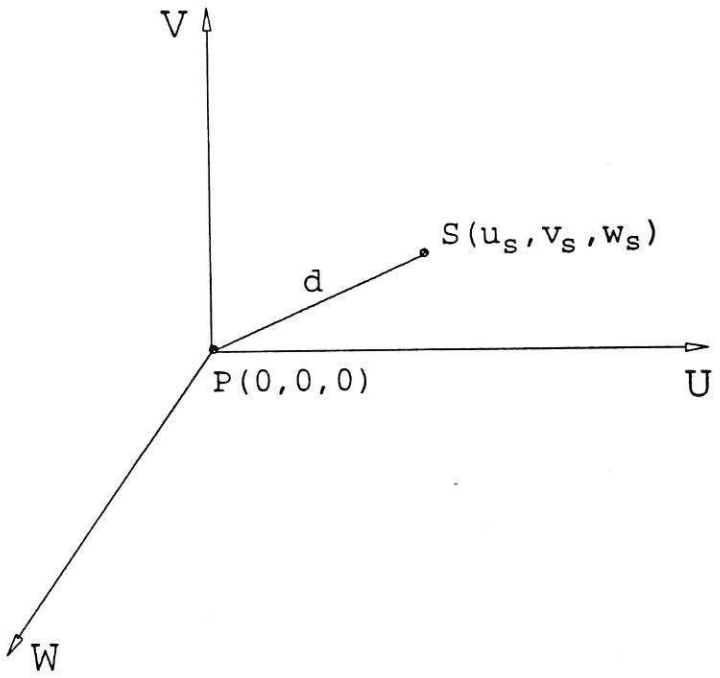

Fig. 2: Primary and secondary sources
in three-dimensional coordinates.

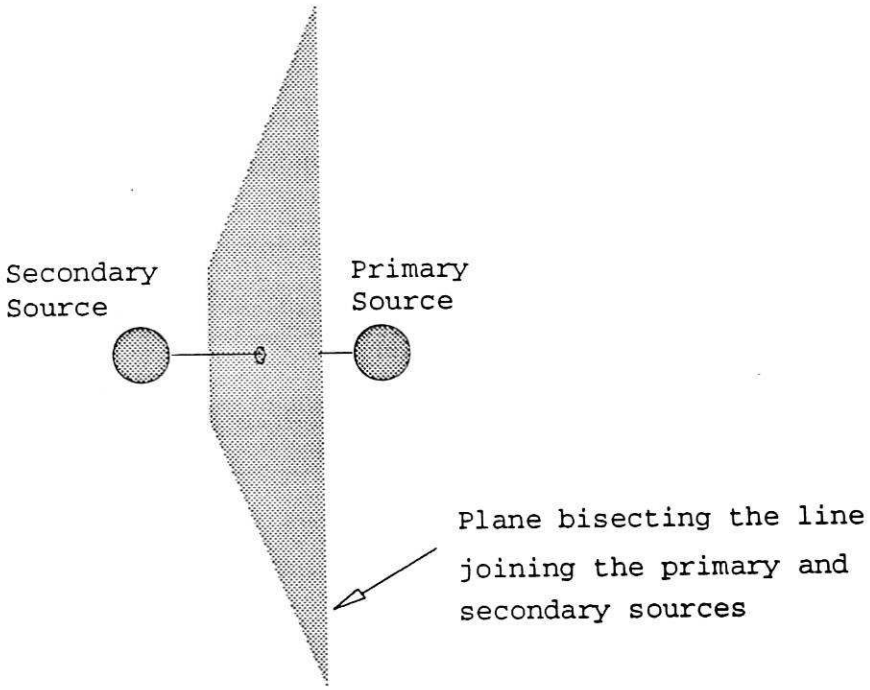

Fig. 3: Plane of the infinite-gain controller.

Non–unity distance ratio

For a non-unity distance ratio equation (6) yield

$$\frac{r_e}{r_f} = a \quad , \quad \frac{r_g}{r_h} = a \quad \text{and} \quad \frac{r_e}{r_g} = 1 \tag{8}$$

It follows from Appendix A that the first two relations in equation (8) define a spherical surface. For the primary and secondary sources located as in Fig. 2 in a three-dimensional *UVW*–space this surface is defined by

$$\left[u + \frac{a^2 u_s}{1 - a^2} \right]^2 + \left[v + \frac{a^2 v_s}{1 - a^2} \right]^2 + \left[w + \frac{a^2 w_s}{1 - a^2} \right]^2 = \left[\frac{ad}{1 - a^2} \right]^2 \tag{9}$$

which has a radius $R = \dfrac{ad}{|\,1 - a^2\,|}$ and centre located along the line PS, joining the primary and secondary source locations, at the point $Q\,(-\dfrac{a^2 u_s}{1 - a^2} , -\dfrac{a^2 v_s}{1 - a^2} , -\dfrac{a^2 w_s}{1 - a^2})$.

The third relation in equation (8) requires the equality of the distances between the detector and primary source, r_e, and between the observer and primary source, r_g. The locus of such points in the three-dimensional *UVW*–space of Fig. 2 (for, say, constant r_e) is a sphere with centre at the primary source location and radius equal to r_e;

$$u^2 + v^2 + w^2 = r_e^{\,2} \tag{10}$$

Therefore, the locus of points defined by equation (8) is given by the intersection of the two spheres in equations (9) and (10). Such a locus is a circle in a plane at right angles with the line joining the centres of the spheres. The centre of the circle, hereafter referred to as the infinite-gain controller (IGC) circle, is also located on this line. Since the centres of the two spheres are located along the line PS joining the primary and secondary source locations the centre of the IGC circle is also located along the line PS.

To investigate the variation of the IGC circle in terms of its radius and location of

its centre in the three-dimensional *UVW*–space of Fig. 2, let the detector be located at point E with coordinates (u_e, v_e, w_e) and distances r_e and r_f relative to the primary and secondary sources respectively. Solving equations (9) and (10) gives the plane of the IGC circle as

$$\frac{u}{(\frac{B}{u_s})} + \frac{v}{(\frac{B}{v_s})} + \frac{w}{(\frac{B}{w_s})} = 1 \qquad (11)$$

where

$$B = \frac{1}{2}\left[d^2 - (\frac{1}{a^2} - 1)\, r_e^2 \right] = \frac{1}{2}\left[d^2 - (r_f^2 - r_e^2) \right] \qquad (12)$$

Equation (11) defines a plane surface on which the IGC circle is residing. The line PS passing through the primary and secondary source locations is found to be at right angles with the plane of IGC circle (see Appendix A). This is shown in two dimensions in Fig. 4a. The corresponding IGC circle is shown in Fig. 4b where r_c is the radius of the IGC circle.

The quantity B in equation (12) gives a measure of the intersection of the plane in equation (11) with the coordinate axes and, thereby, with the line PS passing through the primary and secondary source locations. It follows from equation (12) that B is dependent on d, r_e and r_f or, for constant d, B is dependent on the detector location in the three-dimensional medium. If θ denotes the angle between the lines PE and PS in a plane formed by these lines, Fig. 4c, then equation (12) yields

$$B = r_e d\cos\theta \quad , \quad 0 \le \theta \le \pi$$

from which it follows that as the detection point changes position in the medium the limits for B are found to be

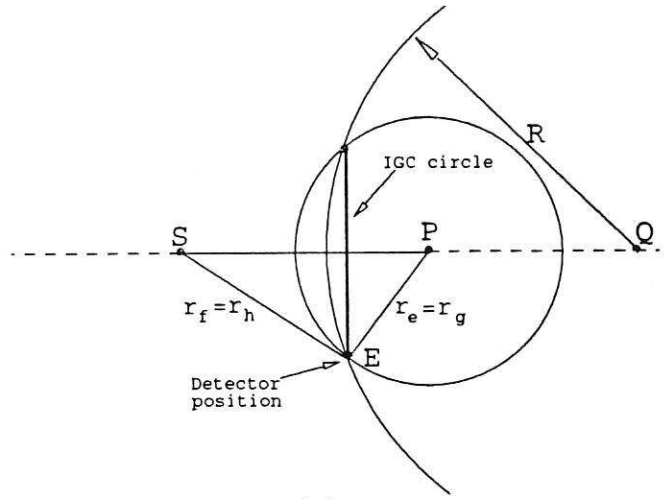

(a)

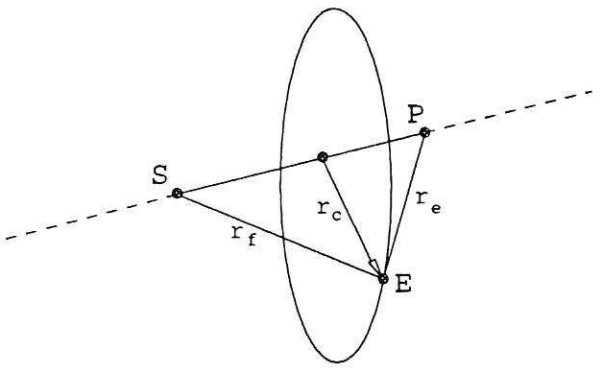

(b)

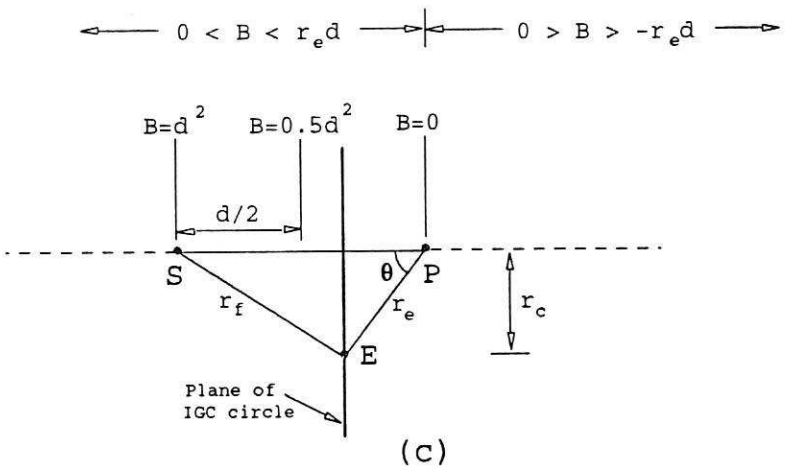

(c)

Fig. 4: The infinite-gain controller circle;
(a) Formation,
(b) IGC circle,
(c) Position with detector location.

$$| B | \leq r_e d$$

This variation in relation to the location of the plane of the IGC circle is shown in two dimensions in Fig. 4c.

From Fig. 4c the radius r_c of the IGC circle can be written as

$$r_c = r_e \sin\theta \quad , \quad 0 \leq \theta \leq \pi \tag{13}$$

It follows from equation (13) that the IGC circle has a radius r_c that is dependent on the distance r_e between the primary source and the detector and the sine of the angle formed by the line joining the primary source and detector with the line joining the primary and secondary sources. The maximum value of the radius, $r_{c\,max}$, is r_e and occurs at the situation where the plane of IGC circle intersects the line PS at point P (Fig. 4c);

$$r_{c\,max} = r_e$$

For a movement of the plane to either side of point P the radius decreases. At the extreme cases where the line PE is in alignment with the line PS (θ is either 0° or 180°) the radius r_c is zero. In general, for constant values of the angle θ the radius r_c is directly proportional to the distance r_e between the primary source and the detector. This implies that for r_c to be minimized the detector is required to be placed as close to the primary source as possible.

An example of the IGC requirement is when, in Fig. 1b, $E(s) = G(s)$ and $F(s) = H(s)$. This corresponds to the feedback control structure first proposed by Olson and later investigated by others [25-31]. In this structure the detector and observer locations happen to coincide with a single point on the IGC circle.

4 System stability

As noted in Fig. 1b the loop formed by the detector, controller, secondary source and the acoustic path between the secondary source and the detector is the only feedback loop present in this structure and may cause instability in the system response. This is due to the acoustic feedback from the secondary source radiation towards the detector. Therefore, from a stability point of view, it is sufficient to concentrate the analysis to this part of the system. Fig. 5 shows a block diagram of this loop where $P_m(s)$ is the primary signal as measured at the point of detection and $S(s)$ is the secondary source output signal. The controller transfer function $C(s)$ in Fig. 5 is assumed to be the required transfer function for optimum cancellation, equation (2).

From the block diagram in Fig. 5 the secondary signal $S(s)$ can be written as

$$S(s) = M(s)C(s)N(s)L(s)\left[P_m(s) + F(s)S(s)\right]$$

Simplifying this for the transfer function between $P_m(s)$ and $S(s)$ yields

$$\frac{S(s)}{P_m(s)} = \frac{M(s)C(s)N(s)L(s)}{1 + X(s)} \tag{14}$$

where

$$X(s) = -M(s)C(s)N(s)L(s)F(s) \tag{15}$$

Equation (14) has been written in a form to correspond to the standard negative feedback transfer function. It follows from this equation that for the system in Fig. 5 to be stable the denominator, $1 + X(s)$, should have roots in the left-hand-side of the s–plane [32]. Note that equation (14) holds only if the primary source output is observable; i.e. the detector is not located at a pressure null in the primary sound field.

4.1 *The Nyquist stability criterion*

The Nyquist stability criterion is a graphical method for determining the stability of the system [32]. It is expressed in terms of the polar plot of the transfer function $X(s)$ for periodic waves ($s = j\omega$). Let $X(j\omega)$ have a magnitude $B(\omega)$ and a phase $\theta(\omega)$;

$$X(j\omega) = B(\omega)\, e^{j\theta(\omega)} \tag{16}$$

Then it follows from the Nyquist stability criterion that for the system in Fig. 5 and hence the ANC structure in Fig. 1 to be stable the magnitude of $X(j\omega)$ at some frequency ω for which $\theta(\omega) = -(2n + 1)\pi$, $n = 0, 1, 2, \cdots$, should be less than unity [32];

$$B(\omega) < 1 \quad \text{when} \quad \theta(\omega) = -(2n + 1)\pi \quad , \; n = 0, 1, 2, \cdots \tag{17}$$

where the negative angle (clockwise) indicates the direction of approach towards the π axis on a polar plot of $X(j\omega)$. This can be expressed graphically by following the polar plot of $X(j\omega)$ from $\omega = 0$ to $\omega = \infty$ and observing each crossing of the π axis. If the point -1 lies on the left-hand-side then the system is considered to be stable whereas if the point -1 lies on the right-hand-side then the system is unstable.

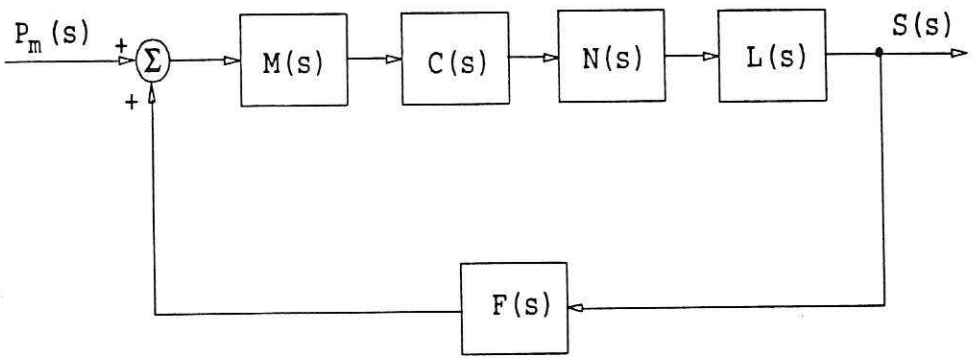

Fig. 5: Feedback loop in the FFCS.

4.1.1 Gain and phase margins

For practical systems a measure of absolute stability is not useful; a system that has an extremely long and oscillatory transient is unlikely to be accepted. In this respect a measure of the relative stability can provide a more acceptable design criterion. This, using frequency response plots, can be provided in terms of the gain and phase margins.

The gain margin is defined, at some frequency ω for which the phase $\theta(\omega)$ is $-180°$, as the additional gain k_g required to make the system unstable. In terms of the amplitude transfer function $B(\omega)$, k_g is given by

$$k_g = \frac{1}{B(\omega)} \quad \text{when} \quad \theta(\omega) = -\pi \tag{18}$$

Thus, it follows from equations (17) and (18) that for a system to be stable the gain margin k_g must be greater than unity. A gain margin less than unity will mean that the system is unstable.

The phase margin is defined, at some frequency ω for which $B(\omega) = 1$, as the additional phase k_θ that is required to make the system unstable. This in terms of the phase $\theta(\omega)$ is given by

$$k_\theta = \theta(\omega) + \pi \quad \text{when} \quad B(\omega) = 1 \tag{19}$$

Thus, it follows from equations (17) and (19) that the phase margin k_θ at a frequency ω for which $B(\omega) = 1$ is the amount of phase shift that would just produce instability. For minimum-phase systems to be stable the phase margin must be positive. A negative phase margin will mean that the system is unstable.

4.2 *Required controller transfer function*

Let the controller in Fig. 5 have the required transfer function for optimum cancellation of noise, as given in equation (2). Substituting for $C(s)$ from equation (2) into equation (15), using equation (3), and simplifying yields

$$X(s) = \frac{1}{\frac{E(s)H(s)}{F(s)G(s)} - 1}$$

For periodic waves ($s = j\omega$) this yields

$$X(j\omega) = \frac{1}{Q(\omega)\ e^{j\phi(\omega)} - 1} \tag{20}$$

where

$$\frac{E(j\omega)H(j\omega)}{F(j\omega)G(j\omega)} = Q(\omega)\ e^{j\phi(\omega)} \tag{21}$$

Simplification of equation (20) yields the magnitude $B(\omega)$ and phase $\theta(\omega)$ of $X(j\omega)$ as

$$\begin{aligned} B(\omega) &= \left[Q^2(\omega) + 1 - 2Q(\omega)cos\phi(\omega) \right]^{-\frac{1}{2}} \\ \theta(\omega) &= \tan^{-1}\left[\frac{Q(\omega)\ \sin\phi(\omega)}{1 - Q(\omega)\ \cos\phi(\omega)} \right] + 2m\pi \quad , \ m = 0, \pm 1, \cdots \end{aligned} \tag{22}$$

To relate the stability of the system to the geometrical arrangement of the ANC system in a three-dimensional non-dispersive propagation medium, let the primary and secondary sources, as shown in Fig. 6, be located in a three-dimensional *UVW*–space at points $P\ (\ 0, 0, 0\ )$ and $S\ (\ u_s\ ,\ v_s\ ,\ w_s\ )$, respectively, a distance d apart, the detector at point $D\ (\ u_d\ ,\ v_d\ ,\ w_d\ )$ with distances r_e and r_f from the primary and secondary sources respectively and the observer at point $O\ (\ u_o\ ,\ v_o\ ,\ w_o\ )$ with distances r_g and r_h from the primary and secondary sources respectively. Thus,

$$r_e = \left[u_d^2 + v_d^2 + w_d^2 \right]^{\frac{1}{2}}$$

$$r_f = \left[(u_d - u_s)^2 + (v_d - v_s)^2 + (w_d - w_s)^2 \right]^{\frac{1}{2}} \tag{23}$$

$$r_g = \left[u_o^2 + v_o^2 + w_o^2 \right]^{\frac{1}{2}}$$

$$r_h = \left[(u_o - u_s)^2 + (v_o - v_s)^2 + (w_o - w_s)^2 \right]^{\frac{1}{2}} \tag{24}$$

and

$$d = \left[u_s^2 + v_s^2 + w_s^2 \right]^{\frac{1}{2}} \tag{25}$$

Substituting for $E(j\omega)$, $F(j\omega)$, $G(j\omega)$, and $H(j\omega)$ from equation (5) into equation (21) and simplifying yields $Q(\omega)$ and $\phi(\omega)$ as

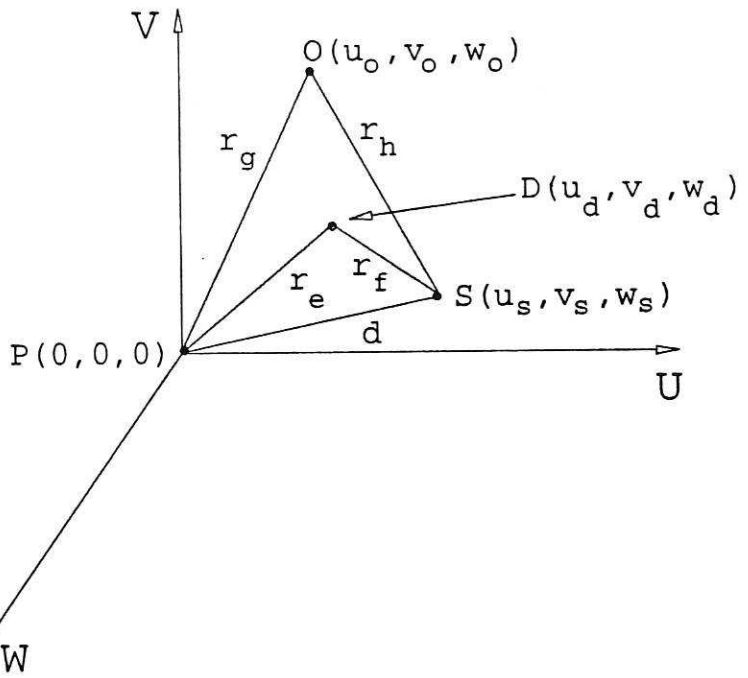

Fig. 6: Components of a FFCS in 3-D coordinates.

$$Q(\omega) = \frac{r_f r_g}{r_e r_h} = \frac{(\frac{r_g}{r_h})}{(\frac{r_e}{r_f})}$$

$$\phi(\omega) = \frac{2\pi}{\lambda}\left[(r_h - r_g) - (r_f - r_e)\right] = \frac{2\pi}{\lambda}(r_{gh} - r_{ef}) \tag{26}$$

where $r_{ef} = r_f - r_e$ and $r_{gh} = r_h - r_g$.

Equations (26) give the magnitude $Q(\omega)$ and phase $\phi(\omega)$ in terms of the distances r_e, r_f, r_g, r_h and the signal wavelength only. Using these relations the stability of the ANC system can be determined in terms of the locations of the detector and observer with respect to the primary and secondary sources in the three-dimensional propagation medium.

4.2.1 Gain margin

Substituting for $\theta(\omega)$ from equation (22) into equation (18) yields

$$\tan^{-1}\left[\frac{Q(\omega)sin\phi(\omega)}{1 - Q(\omega)cos\phi(\omega)}\right] + 2m\pi = -\pi \quad , \; m = 0, \pm 1, \cdots$$

or

$$\frac{Q(\omega)sin\phi(\omega)}{Q(\omega)cos\phi(\omega) - 1} = \tan(2m + 1)\pi \quad , \; m = 0, \pm 1, \cdots$$

from which it follows that the following conditions should hold

$$Q(\omega)sin\phi(\omega) = 0$$

$$Q(\omega)cos\phi(\omega) - 1 < 0$$

Since $Q(\omega)$ is strictly a positive real number the above equations reduce to

$$\begin{aligned} \sin\phi(\omega) = 0 \ , \quad \cos\phi(\omega) = +1 \quad \text{and} \quad Q(\omega) < 1 \\ \sin\phi(\omega) = 0 \ , \quad \cos\phi(\omega) = -1 \quad \text{and} \quad Q(\omega) > 0 \end{aligned} \tag{27}$$

where in the second of equation (27) $Q(\omega) > -1$ is replaced by $Q(\omega) > 0$ to correspond with its realistic range.

Simplifying equation (27) yields the angle $\phi(\omega)$ as

$$\phi(\omega) = \begin{cases} 2n\pi & \text{for} \quad Q(\omega) < 1 \\ (2n+1)\pi & \text{for} \quad Q(\omega) > 0 \end{cases} \ , \ n = 0, \pm 1, \cdots$$

or

$$\phi(\omega) = \begin{cases} (2n+1)\pi & \text{for} \quad Q(\omega) \geq 1 \\ n\pi & \text{for} \quad 0 < Q(\omega) < 1 \end{cases} \ , \ n = 0, \pm 1, \cdots \tag{28}$$

Substituting for $\phi(\omega)$ from equation (26) into equation (28) and simplifying yields

$$r_{gh} - r_{ef} = \begin{cases} (2n+1)\,\dfrac{\lambda}{2} & \text{for} \quad Q(\omega) \geq 1 \\ n\,(\dfrac{\lambda}{2}) & \text{for} \quad 0 < Q(\omega) < 1 \end{cases} \ , \ n = 0, \pm 1, \cdots \tag{29}$$

Equations (28) and (29) give the necessary conditions under which the phase $\theta(\omega)$ of the transfer function $X(j\omega)$ is -180°. In this case the gain margin k_g of the system is given by equation (18).

Substituting for $\phi(\omega) = 2n\pi$ into equation (22) and using equation (18) yields, after simplification, the gain margin as

$$k_g = \left[Q^2(\omega) + 1 - 2\,Q(\omega) \right]^{\frac{1}{2}} = |\, Q(\omega) - 1 \,|$$

As it follows from equation (28) that $Q(\omega)$ is to be less than unity for this case, the above equation simplifies to

$$k_g = 1 - Q(\omega) \quad \text{for} \quad 0 < Q(\omega) < 1 \quad \text{and} \quad \phi(\omega) = 2n\pi \quad , \; n = 0, \pm 1, \cdots \tag{30}$$

If $\phi(\omega) = (\, 2n + 1 \,)\pi$ then equations (18) and (22) yield the gain margin as

$$k_g = \left[\, Q^2(\omega) + 1 + 2 \, Q(\omega) \, \right]^{\frac{1}{2}} = | \, Q(\omega) + 1 \, |$$

and as in this case $Q(\omega)$ is greater than zero, equation (28) shows that the above equation simplifies to

$$k_g = Q(\omega) + 1 \quad \text{for} \quad Q(\omega) > 0 \quad \text{and} \quad \phi(\omega) = (\, 2n + 1 \,)\pi \quad , \; n = 0, \pm 1, \cdots \tag{31}$$

Combining equations (30) and (31) yields the gain margin as

$$k_g = \begin{cases} 1 - Q(\omega) & \text{for} \quad \phi(\omega) = 2n\pi \quad \text{and} \quad 0 < Q(\omega) < 1 \\ 1 + Q(\omega) & \text{for} \quad \phi(\omega) = (\, 2n + 1 \,)\pi \quad \text{and} \quad Q(\omega) > 0 \end{cases} \tag{32}$$

where $n = 0, \pm 1, \cdots$.

Using Nyquist's stability criterion, defined in equation (17), it may be concluded that for stable operation of the system the gain margin should assume values greater than unity;

$$k_g > 1 \tag{33}$$

To find the specified regions in the three-dimensional *UVW*–space of Fig. 6 corresponding to equation (32) and analyze system stability in these regions consider the two cases of $Q(\omega) \geq 1$ and $Q(\omega) < 1$.

$Q(\omega)$ greater than or equal unity

Substituting for $Q(\omega) \geq 1$ into equation (26) and simplifying yields

$$\frac{r_e}{r_f} \leq a \tag{34}$$

where a is a positive real number denoting the distance ratio $\frac{r_g}{r_h}$;

$$a = \frac{r_g}{r_h} \tag{35}$$

It follows from Appendix A that the distance ratio a in equation (35) defines a family of spheres in the three-dimensional *UVW*–space of Fig. 6. Substituting into equation (35) for r_g and r_h from equation (24), using equation (25), and simplifying yields the locus of points $O\ (u_o\ ,\ v_o\ ,\ w_o\ )$ in Fig. 6 defined as

$$\left[u_o + \frac{a^2\, u_s}{1 - a^2} \right]^2 + \left[v_o + \frac{a^2\, v_s}{1 - a^2} \right]^2 + \left[w_o + \frac{a^2\, w_s}{1 - a^2} \right]^2 = \left[\frac{ad}{1 - a^2} \right]^2 \tag{36}$$

This expression for a distance ratio a equal to zero corresponds to point P (location of the primary source) and for an infinitely large distance ratio to point S (location of the secondary source). If the distance ratio is equal to unity then equation (36) defines a plane surface that perpendicularly bisects the line PS joining the locations of the primary and secondary sources;

$$\frac{u_o}{(\frac{d^2}{2u_s})} + \frac{v_o}{(\frac{d^2}{2v_s})} + \frac{w_o}{(\frac{d^2}{2w_s})} = 1 \tag{37}$$

It follows from the above that for $Q(\omega) \geq 1$ the detection point in Fig. 6 should remain inside the sphere defined by equation (36). In terms of the distance ratio a, this means that for $a < 1$ the locus of points $D\ (u_d\ ,\ v_d\ ,\ w_d\ )$ in Fig. 6 should define the region on and inside the sphere in equation (36); for $a = 1$ point D should be on and in the region on the side of the plane defined by equation (37) that contains point P; and for $a > 1$ point D should be on and outside the sphere defined by equation (36). Substituting for r_e and r_f from equation (23) into equation (34), using equation (25), and simplifying gives for the above cases:

$$\left[u_d + \frac{a^2 u_s}{1-a^2}\right]^2 + \left[v_d + \frac{a^2 v_s}{1-a^2}\right]^2 + \left[w_d + \frac{a^2 w_s}{1-a^2}\right]^2 \leq \left[\frac{ad}{1-a^2}\right]^2 \quad , \; a < 1$$

$$\frac{u_d}{\left(\frac{d^2}{2u_s}\right)} + \frac{v_d}{\left(\frac{d^2}{2v_s}\right)} + \frac{w_d}{\left(\frac{d^2}{2w_s}\right)} \leq 1 \quad , \; a = 1 \tag{38}$$

$$\left[u_d - \frac{a^2 u_s}{a^2-1}\right]^2 + \left[v_d - \frac{a^2 v_s}{a^2-1}\right]^2 + \left[w_d - \frac{a^2 w_s}{a^2-1}\right]^2 \geq \left[\frac{ad}{a^2-1}\right]^2 \quad , \; a > 1$$

This is shown in two dimensions in Fig. 7, where the shaded regions indicate the detector locations D.

It follows from the preceding discussion that if the observer O and detector D are restricted to the regions of the UVW–space defined by equations (36) and (38) respectively, then the gain $Q(\omega)$ will be greater than or equal to unity. In terms of equations (29) and (32) this means that for such observation and detection points where the distance difference $r_{gh} - r_{ef}$ is an odd multiple of half the signal wavelength (implying that the angle $\phi(\omega)$ is an odd multiple of π and the angle $\theta(\omega)$ in equation (16) is -180°) the gain margin k_g of the system in Fig. 7 is given by equation (32) as

$$k_g = 1 + Q(\omega) \quad \text{for} \quad \phi(\omega) = (2n+1)\pi \quad \text{and} \quad Q(\omega) \geq 1 \tag{39}$$

where $n = 0, \pm 1, \cdots$.

It follows from equation (39) that under this situation the gain margin assumes values that are either equal to or greater than 2;

$$k_g \geq 2 \quad \text{for} \quad \phi(\omega) = (2n+1)\pi \quad \text{and} \quad Q(\omega) \geq 1$$

Using the condition for stability of the system given in equation (33) implies that if the observer and detector are restricted to the regions defined by equations (36) and (38) of the three-dimensional UVW–space of Fig. 6 then at locations for which $\phi(\omega)$ is an odd multiple of π (the feedback loop in Fig. 5 having a phase $\theta(\omega) = -180^\circ$) the system will

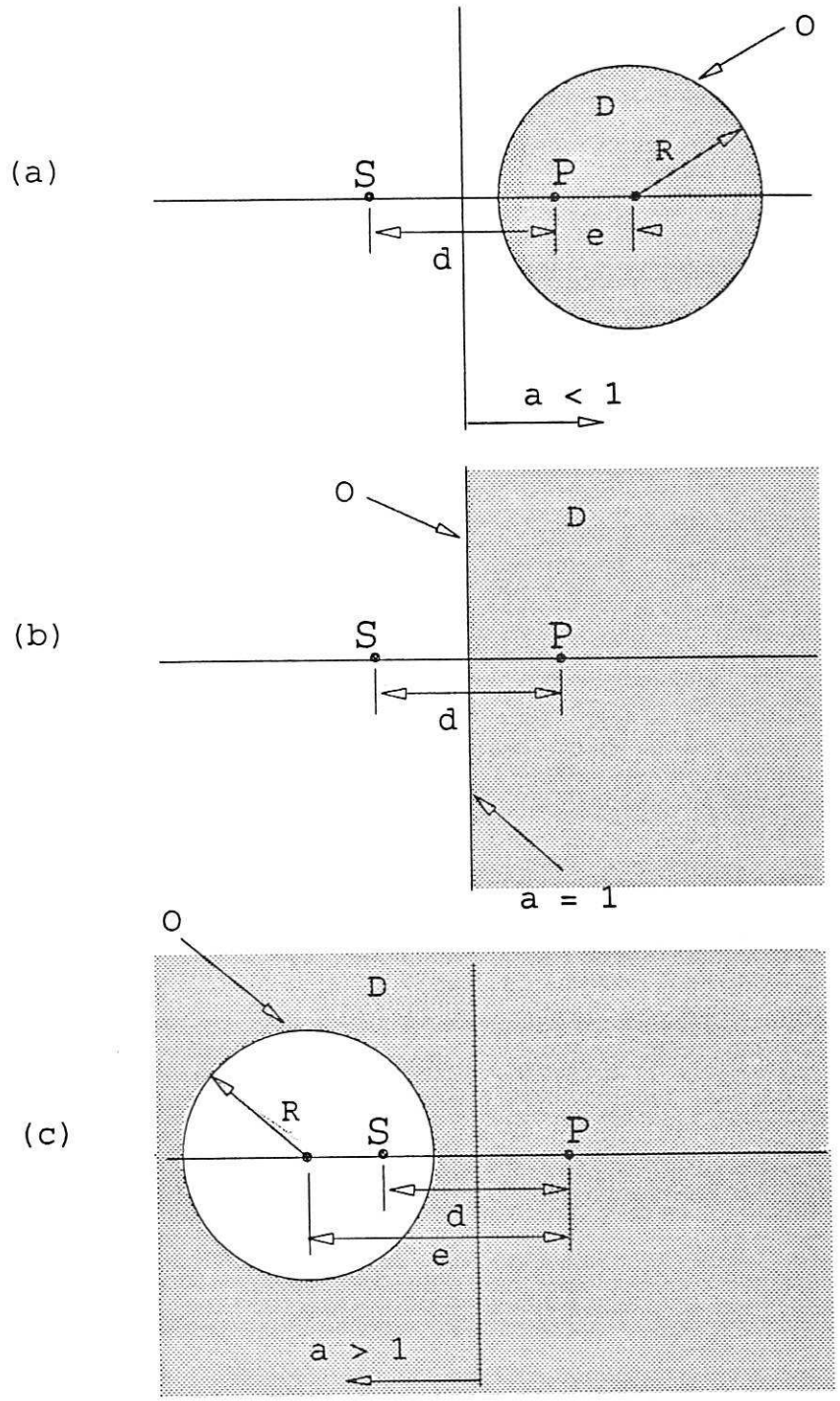

$$\left[\ e=\frac{a^2 d}{|a^2-1|}\ \text{ and }\ R=\frac{e}{a}\ \right]$$

Fig. 7: Region of observer O and detector D for $Q \geq 1$.

be stable.

$Q(\omega)$ less than unity

Substituting for $Q(\omega) < 1$ into equation (26) and using equation (35) yields

$$\frac{r_e}{r_f} > a \tag{40}$$

It follows from the results obtained above for $Q(\omega) \geq 1$ that equation (40), for points of observation O and detection D, defines a region of the three-dimensional UVW–space in Fig. 6 which is the complement of that given in equations (36) and (38); i.e. for the observer restricted to the locus defined by equation (36) the detector is to be restricted to the following

$$\left[u_d + \frac{a^2 u_s}{1-a^2}\right]^2 + \left[v_d + \frac{a^2 v_s}{1-a^2}\right]^2 + \left[w_d + \frac{a^2 w_s}{1-a^2}\right]^2 > \left[\frac{ad}{1-a^2}\right]^2 \quad , \; a < 1$$

$$\frac{u_d}{\left(\frac{d^2}{2u_s}\right)} + \frac{v_d}{\left(\frac{d^2}{2v_s}\right)} + \frac{w_d}{\left(\frac{d^2}{2w_s}\right)} > 1 \quad , \; a = 1 \tag{41}$$

$$\left[u_d - \frac{a^2 u_s}{a^2-1}\right]^2 + \left[v_d - \frac{a^2 v_s}{a^2-1}\right]^2 + \left[w_d - \frac{a^2 w_s}{a^2-1}\right]^2 < \left[\frac{ad}{a^2-1}\right]^2 \quad , \; a > 1$$

This is shown in two dimensions in Fig. 8 where the shaded areas indicate the detector locations D.

If the observer and detector are restricted to their respective regions defined by equations (36) and (41), then at locations for which the distance difference $r_{gh} - r_{ef}$ (defined in equation (29)) is an integral multiple of the signal wavelength (implying that the angle $\phi(\omega)$ is an integral multiple of π and the phase $\theta(\omega)$ in equation (16) will be -180°) the gain margin of the system in Fig. 5 is given by equation (32) as

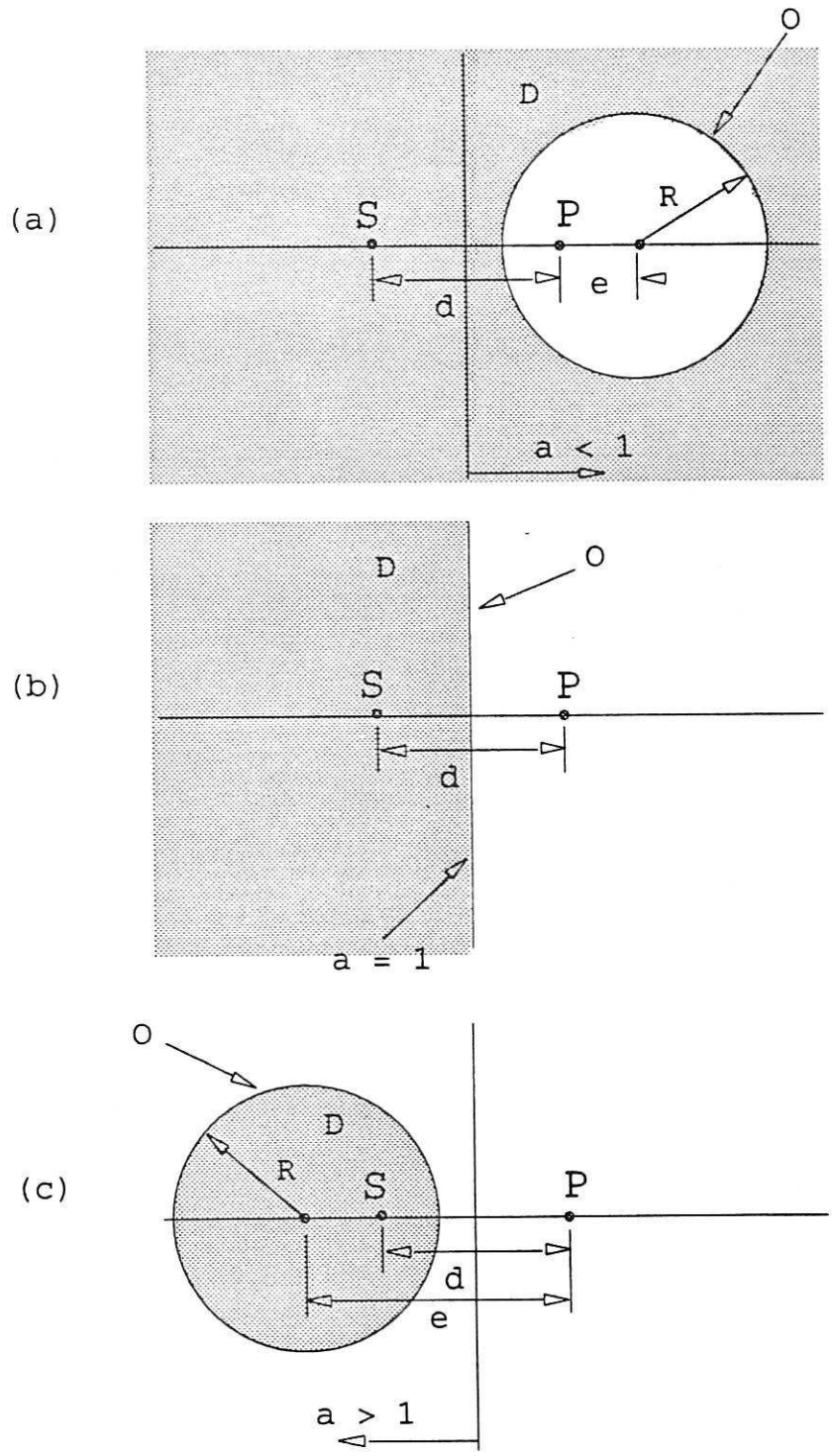

$$\left[\ e=\frac{a^2 d}{|a^2-1|}\ \text{ and }\ R=\frac{e}{a}\ \right]$$

Fig. 8: Region of observer O and detector D for Q<1.

$$k_g = \begin{cases} 1 - Q(\omega) & \text{for} \quad \phi(\omega) = 2n\pi \\ 1 + Q(\omega) & \text{for} \quad \phi(\omega) = (2n+1)\pi \end{cases} \qquad n = 0, \pm 1, \cdots$$

From which the ranges of the gain margin are obtained as

$$\begin{matrix} k_g < 1 & \text{for} \quad \phi(\omega) = 2n\pi \\ k_g > 1 & \text{for} \quad \phi(\omega) = (2n+1)\pi \end{matrix} \quad , \; n = 0, \pm 1, \cdots \tag{42}$$

Equation (42) when compared with equation (33) implies that for such detection and observation points in the region of the three-dimensional *UVW*–space defined by equation (40) for which $\phi(\omega)$ is an even multiple of π, the gain margin of the feedback loop in Fig. 5 is less than unity and hence the system will be unstable. However, if at such points $\phi(\omega)$ is an odd multiple of π, then the gain margin is greater than unity and hence in such a situation the system will be stable.

4.2.2 Phase margin

The phase margin, k_θ, of the feedback loop in Fig. 5 is given by equation (19). Substituting for $B(\omega)$ from equation (22) into equation (19) yields

$$\left[Q^2(\omega) + 1 - 2\, Q(\omega) \cos\phi(\omega) \right]^{-\frac{1}{2}} = 1$$

Simplifying this yields

$$\cos\phi(\omega) = \frac{Q(\omega)}{2} \tag{43}$$

The amplitude $Q(\omega)$ is strictly a positive quantity; moreover, for $\phi(\omega)$ to have a realistic value satisfying equation (43), $Q(\omega)$ should not exceed 2;

$$0 < Q(\omega) \leq 2 \tag{44}$$

Equations (43) and (44) yield the range of $\phi(\omega)$ as

$$\frac{(4n-1)\pi}{2} < \phi(\omega) < \frac{(4n+1)\pi}{2} \quad \text{for} \quad 0 < Q(\omega) \leq 2 \quad , \; n = 0, \pm 1, \cdots \tag{45}$$

Substituting for $\phi(\omega)$ from equation (26) into equation (45), and simplifying yields the allowable distance difference $r_{gh} - r_{ef}$ as

$$(4n-1)\frac{\lambda}{4} < r_{gh} - r_{ef} < (4n+1)\frac{\lambda}{4} \quad \text{for} \quad 0 < Q(\omega) \leq 2 \quad , \; n = 0, \pm 1, \cdots \tag{46}$$

Equation (46), or equivalently equation (42), is the necessary condition for $B(\omega) = 1$ in equation (19). Under this condition the phase angle $\theta(\omega)$ follows from equation (22). Using equations (43) and (45) the following is obtained

$$\sin\phi(\omega) = \begin{cases} \frac{1}{2}\sqrt{4 - Q^2(\omega)} & \text{for} \quad 0 \leq \phi(\omega) < \frac{(4n+1)\pi}{2} \\ -\frac{1}{2}\sqrt{4 - Q^2(\omega)} & \text{for} \quad \frac{(4n-1)\pi}{2} < \phi(\omega) < 0 \end{cases} \quad , \; 0 < Q(\omega) \leq 2 \tag{47}$$

where $n = 0, \pm 1, \cdots$. Substituting for $\cos\phi(\omega)$ and $\sin\phi(\omega)$ from equations (43) and (47) into equation (22) and simplifying yields the phase angle $\theta(\omega)$ as

$$\theta(\omega) = \begin{cases} \tan^{-1}\frac{Q(\omega)\sqrt{4 - Q^2(\omega)}}{2 - Q^2(\omega)} + 2m\pi & \text{for} \quad 0 \leq \phi(\omega) < \frac{(4n+1)\pi}{2} \\ -\tan^{-1}\frac{Q(\omega)\sqrt{4 - Q^2(\omega)}}{2 - Q^2(\omega)} + 2m\pi & \text{for} \quad \frac{(4n-1)\pi}{2} < \phi(\omega) < 0 \end{cases} \tag{48}$$

where $0 < Q(\omega) \leq 2$, $m = 0, \pm 1, \cdots$ and $n = 0, \pm 1, \cdots$. This is shown as a function of $Q(\omega)$ in Fig. 9a (for $m = 0$).

Substituting for $\theta(\omega)$ from equation (48) into equation (19) yields the gain margin as

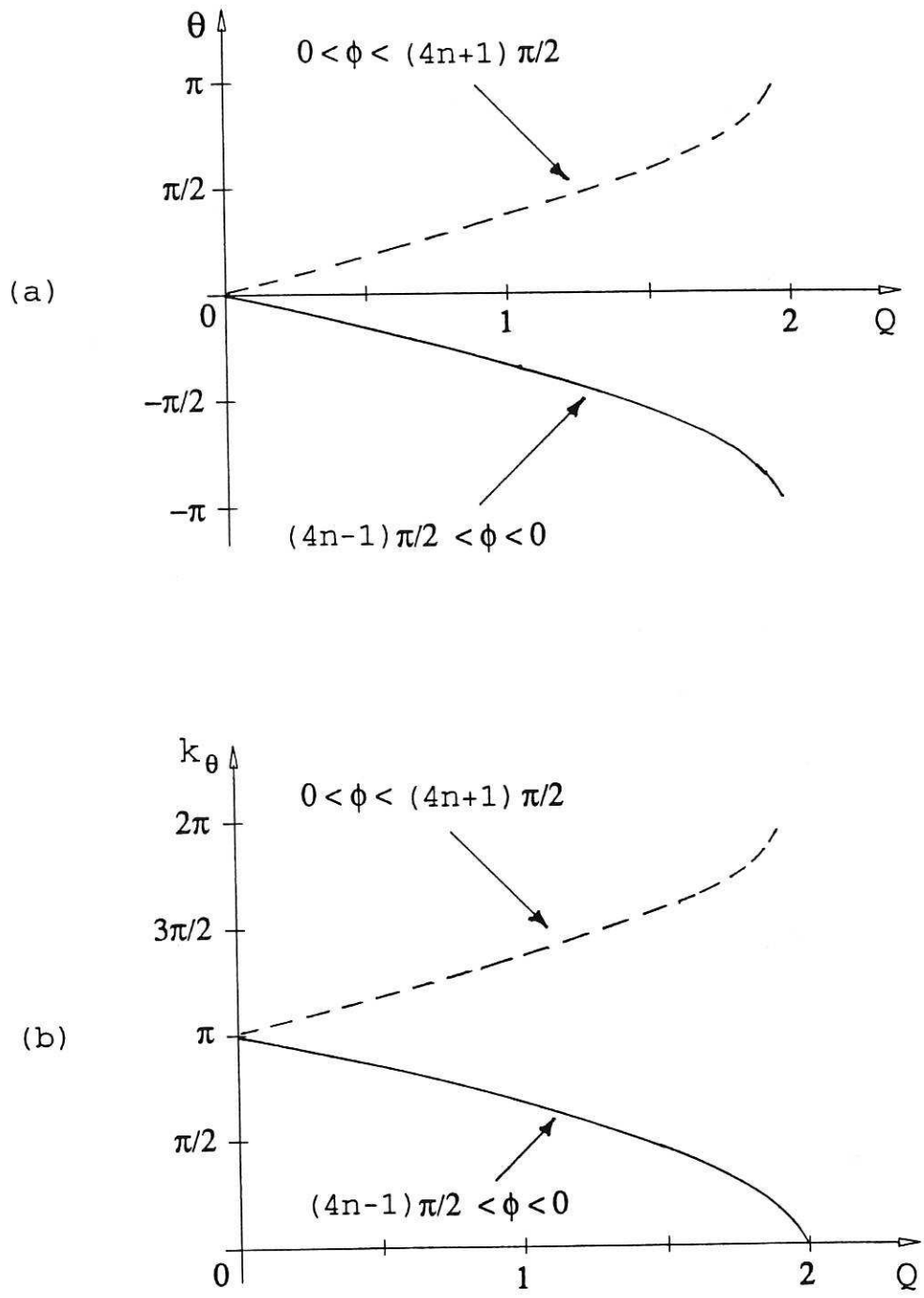

Fig. 9: (a) Phase, (b) Phase margin of the feedback loop.

$$k_\theta = \begin{cases} \tan^{-1} \dfrac{Q(\omega)\sqrt{4 - Q^2(\omega)}}{2 - Q^2(\omega)} + (2m+1)\pi & \text{for } 0 \le \phi(\omega) < \dfrac{(4n+1)\pi}{2} \\ -\tan^{-1} \dfrac{Q(\omega)\sqrt{4 - Q^2(\omega)}}{2 - Q^2(\omega)} + (2m+1)\pi & \text{for } \dfrac{(4n-1)\pi}{2} < \phi(\omega) < 0 \end{cases} \tag{49}$$

where $0 < Q(\omega) \le 2$ and m and n are integer numbers. This, shown as function of $Q(\omega)$ in Fig. 9b (for $m = 0$), is the phase margin of the feedback loop in Fig. 5. To find the corresponding region of the three-dimensional *UVW*–space of Fig. 6 in terms of the locations of the observation and detection points we consider equation (44).

Substituting for $Q(\omega)$ from equation (26) into equation (44) and using equation (35), yields after simplification,

$$\frac{r_e}{r_f} \ge 0.5\, a \tag{50}$$

Substituting for r_e and r_f from equation (23) into equation (50), simplifying, and using equation (25) yields the locus of points $D\,(u_d, v_d, w_d)$ as

$$\left[u_d + \frac{a^2 u_s}{4 - a^2}\right]^2 + \left[v_d + \frac{a^2 v_s}{4 - a^2}\right]^2 + \left[w_d + \frac{a^2 w_s}{4 - a^2}\right]^2 \ge \left[\frac{2\,ad}{4 - a^2}\right]^2 \quad , \; a < 2$$

$$\frac{u_d}{\left(\frac{d^2}{2u_s}\right)} + \frac{v_d}{\left(\frac{d^2}{2v_s}\right)} + \frac{w_d}{\left(\frac{d^2}{2w_s}\right)} \ge 1 \quad , \; a = 2 \tag{51}$$

$$\left[u_d - \frac{a^2 u_s}{a^2 - 4}\right]^2 + \left[v_d - \frac{a^2 v_s}{a^2 - 4}\right]^2 + \left[w_d - \frac{a^2 w_s}{a^2 - 4}\right]^2 \le \left[\frac{2\,ad}{a^2 - 4}\right]^2 \quad , \; a > 2$$

These are shown in two dimensions in Fig. 10.

It follows from the above analysis that for the detector and observer locations, in the region of the three-dimensional *UVW*–space of Fig. 6 defined by equation (44), or equivalently by equation (51), for which equation (43) holds, the amplitude $B(\omega)$ (defined in equation (16)) is unity and in such a case the phase margin k_θ of the feedback loop in

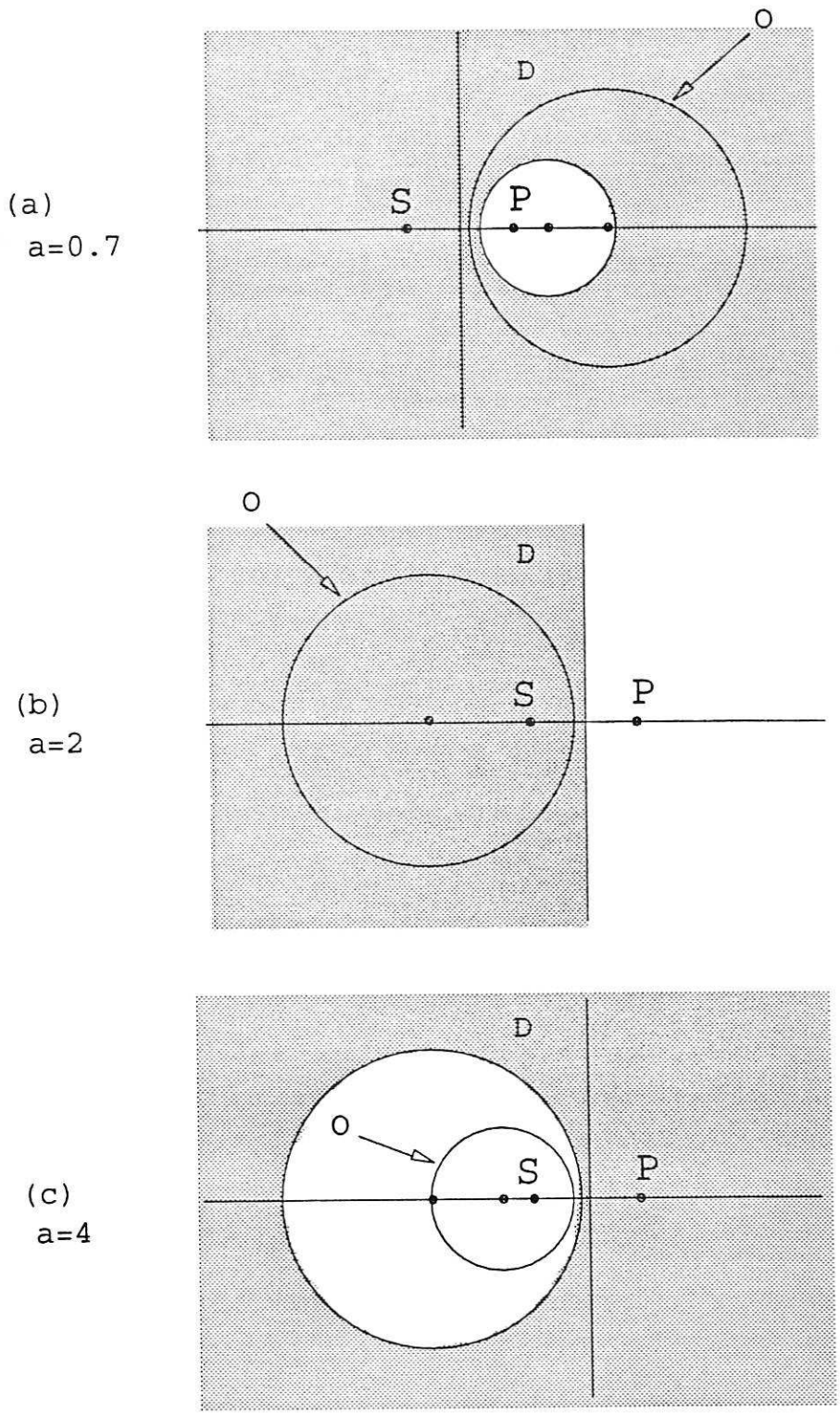

Fig. 10: Region of observer O and detector D for $Q \leq 2$.

Fig. 5 is given by equation (49). In this case, for a minimum-phase situation (all zeros inside the stability region) the system will be stable for locations of detector and observer in the regions defined by equation (51), where the phase margin assumes positive values; however, for negative values of k_θ the system will be unstable.

5 CONCLUSION

An analysis and design procedure for ANC systems under stationary conditions, in a three-dimensional non-dispersive propagation medium, in the general form of a feedforward control structure has been presented and a stability analysis of the system has been given.

Full cancellation over a broad frequency range of an unwanted noise at an observation point in three dimensions requires a controller with a frequency-dependent transfer function that can produce a wave which is an exact mirror image of the noise at the point. The characteristics of such a controller are found to be dependent upon the transfer characteristics of transducers, secondary source and propagation paths from the primary and secondary sources to both the detector and observer locations.

The dependence of controller characteristics, for full cancellation of noise, on the characteristics of system components and geometry can sometimes lead to practical difficulties in the controller design and system stability. A particular combination of these characteristics requires a controller with a particular transfer function. A change in any of these characteristics, such as changing the location of either the detector and/or observer, requires a controller with a new transfer function to suit the new situation. In particular, there are combinations of detector and observer locations which lead to the critical situation of an infinite-gain controller requirement. Moreover, for given system components and controller transfer function the stability and relative stability of the system will be

dependent on the observer and detector locations in the medium. There are combinations of the observation and detection points in the medium which can cause the system to become unstable. However, the region of space that is occupied by the locus of IGC requirement can be minimized as well as stable operation of the system assured by a proper geometrical arrangement of system components.

6 References

1. LUEG. P: 'Process of silencing sound oscillations', US Patent No. 2 043 416, 1936
2. OLSON, H. F. and MAY, E. G.: 'Electronic sound absorber', The Journal of the Acoustical Society of America, 1953, **25**, (6), pp. 1130-1136
3. VOGT, M.: 'General conditions of phase cancellation in an acoustic field', Archives of Acoustics, 1976, **1**, (2), pp. 109-125
4. LEVENTHAL, H. G.: 'Developments in active attenuators', Proceedings of Noise Control Conference, Warsaw, Poland, 13-15 October 1976, pp. 33-42
5. WARNAKA, G. E.: 'Active attenuation of noise: the state of the art', Noise Control Engineering, 1982, **18**, (3), pp. 100-110
6. LEITCH, R. R. and TOKHI, M. O.: 'Active noise control systems', IEE Proceedings, Part A, 1987, **134**, pp. 525-546
7. ROSS, C. F.: 'An algorithm for designing a broadband active sound control system', Journal of Sound and Vibration, 1982, **80**, (3), pp. 373-380
8. CONOVER, W. B.: 'Fighting noise with noise', Noise Control, 1956, **92**, pp. 78-82, 92
9. BURGESS, J. C.: 'Active adaptive sound control in a duct: A computer simulation', The Journal of the Acoustical Society of America, 1981, **70**, (3), pp. 715-726

10. CHAPLIN, B.: 'The cancellation of repetitive noise and vibration', Proceedings of Inter-noise 80: International Conference on Noise Control Engineering, Florida, USA, 8-10 December 1980, **II**, pp. 699-702

11. ROSS, C. F.: 'An adaptive digital filter for broadband active sound control', Journal of Sound and Vibration, 1982, **80**, (3), pp. 381-388

12. ALVAREZ-TINOCO, A. M.: 'Adaptive algorithms for the active attenuation of acoustic noise', Ph.D. Thesis, Heriot-Watt University, Department of Electrical and Electronic Engineering, Edinburgh, UK, November 1985

13. DARLINGTON, P. and ELLIOTT, S. J.: 'Adaptive control of periodic disturbances in resonant systems', Proceedings of the Institute of Acoustics, 1985, **7**, (Part 2), pp. 87-94

14. ELLIOTT, S. J. and NELSON, P. A.: 'An adaptive algorithm for multichannel active control', Proceedings of the Institute of Acoustics, 1986, **8**, (Part 1), pp. 135-147

15. ELLIOTT, S. J., SOTHERS, I. M., and NELSON, P. A.: 'A multiple error LMS algorithm and its application to the active control of sound and vibration', IEEE Transactions on Acoustics, Speech, and Signal Processing, 1987, **ASSP-35**, (10), pp. 1423-1434

16. ERIKSSON, L. J., ALLIE, M. C., and GREINER, R. A. Greiner: 'The selection and application of an IIR adaptive filter for use in active sound attenuation', IEEE Transactions on Acoustics, Speech, and Signal Processing, 1987, **ASSP-35**, (4), pp. 433-437

17. ERIKSSON, L. J., ALLIE, M. C., BREMIGAN, C. D., and GREINER, R. A. Greiner: 'Active noise control using adaptive digital signal processing', Proceedings of the IEEE International Conference on Acoustics, Speech, and Signal Processing,

New York, USA, 1988, **5**, pp. 2594-2597

18. TOKHI, M. O. and LEITCH, R. R.: 'Self-tuning active noise control', IEE Colloquium on Adaptive Filters, London, UK, 22 March 1989

19. JESSEL, M. and MANGIANTE, G. A.: 'Active sound absorbers in an air duct', Journal of Sound and Vibration, 1972, **23**, (3), pp. 383-390

20. KIDO, K.: 'Reduction of noise by use of additional sound sources', Proceedings of Inter-noise 75: International Conference on Noise Control Engineering, Sendai, Japan, 27-29 August 1975, pp. 647-650

21. POOLE, J. and LEVENTHAL, G. H.: 'An experimental study of Swinbanks' method of active attenuation of sound in ducts', Journal of Sound and Vibration, 1976, **49**, (2), pp. 257-266

22. SWINBANKS, M. A.: 'Active control of sound propagation in long ducts', Journal of Sound and Vibration, 1973, **27**, (3), pp. 411-436

23. LEVENTHAL, H. G. and EGHTESADI, Kh.: 'Active attenuation of noise: Monopole and Dipole systems', Proceedings of Inter-noise 79: International Conference on Noise Control Engineering, Warsa, Poland, 11-13 September 1979, **I**, pp. 175-180

24. EGHTESADI, Kh. and LEVENTHAL, H. G.: 'Comparison of active attenuators of noise in ducts', Acoustics Letters, 1981, **4**, (10), pp. 204-209

25. OLSON, H. F.: 'Electronic control of noise, vibration and reverberation', The Journal of the Acoustical Society of America, 1956, **28**, (5), pp. 966-972

26. OLSON, H. F.: 'Electronic sound absorber', US Patent No. 2 983 790, 1961

27. BLEAZY, J. C.: 'Electronic sound absorbers', Journal of Audio Engineering Society, 1962, **10**, (2), pp. 135-139

28. SHORT, W. R.: 'Global low frequency active noise attenuation', Proceedings of

Inter-noise 80: International Conference on Noise Control Engineering, Florida, USA, 8-10 December 1980, **II**, pp. 695-698

29. TRINDER, M. C. J. and NELSON, P. A.: 'The acoustical virtual earth and its application to ducts with reflecting terminations', Proceedings of Inter-noise 83: International Conference on Noise Control Engineering, Edinburgh, UK, 13-15 July 1983, **I**, pp. 447-450

30. TRINDER, M. C. J. and NELSON, P. A.: 'Active noise control in finite length ducts', Journal of Sound and Vibration, 1983, **89**, (1), pp. 95-106

31. CHAPLIN, G. B. B., JONES, A., and JONES, O.: 'Method and apparatus for low frequency active attenuation', US Patent No. 4 527 282, 1985

32. D'AZZO, J. J. and HOUPIS, C. H.: 'Feedback control system analysis and synthesis', (2nd ed), McGraw-Hill, 1966

Appendix A: The locus of constant distance ratio

Theorem A

Let P and S be two fixed points in a three-dimensional space and a distance d apart from each other, and let T be an arbitrary point in this space. If the ratio of the distances PT and ST is constant then the locus of points T defines

(a) a sphere with centre located along the line PS, for a non-unity distance ratio.

(b) a plane perpendicularly bisecting the line PS, for a unity distance ratio.

Proof

Consider a three-dimensional UVW–space with P (0, 0, 0) and S (u_s, v_s, w_s) representing two fixed points and T (u, v, w) an arbitrary point. The distances PS, PT and ST are

respectively denoted by d, r_g and r_h;

$$d = \left[u_s^2 + v_s^2 + w_s^2 \right]^{\frac{1}{2}} \tag{A1}$$

$$\begin{aligned} r_g &= \left[u^2 + v^2 + w^2 \right]^{\frac{1}{2}} \\ r_h &= \left[(u - u_s)^2 + (v - v_s)^2 + (w - w_s)^2 \right]^{\frac{1}{2}} \end{aligned} \tag{A2}$$

Let the distance ratio $\frac{r_g}{r_h}$ be denoted by, a positive real number, a;

$$\frac{r_g}{r_h} = a \tag{A3}$$

This gives the locus of points in the three-dimensional UVW–space that corresponds to a particular distance ratio a.

Non–unity distance ratio

If $a \neq 1$ then substituting for r_g and r_h from equation (A2) into equation (A3), simplifying and using equation (A1) yields

$$\left[u + \frac{a^2 u_s}{1 - a^2} \right]^2 + \left[v + \frac{a^2 v_s}{1 - a^2} \right]^2 + \left[w + \frac{a^2 w_s}{1 - a^2} \right]^2 = \left[\frac{ad}{1 - a^2} \right]^2 \quad , \; a \neq 1 \tag{A4}$$

Equation (A4) represents a sphere with radius $R = \frac{ad}{| 1 - a^2 |}$ and centre at $Q \left(- \frac{a^2 u_s}{1 - a^2}, - \frac{a^2 v_s}{1 - a^2}, - \frac{a^2 w_s}{1 - a^2} \right)$. Through simple mathematical manipulation the point Q is found to be located along the line PS and, specifically, if P is chosen as reference, then for $a > 1$ the centre is located on the portion of PS corresponding to points away from P towards and beyond S whereas for $a < 1$ the centre of the sphere will be on the portion of PS corresponding to points away from P and opposite to S. In either of these situations, point

Q lies outside the range (P, S).

Unity distance ratio

If $a = 1$ then equation (A3) yields

$$r_g = r_h \tag{A5}$$

Substituting for r_g and r_h from equation (A2) into equation (A5), simplifying, and using equation (A1) yields

$$\frac{u}{(\frac{d^2}{2u_s})} + \frac{v}{(\frac{d^2}{2v_s})} + \frac{w}{(\frac{d^2}{2w_s})} = 1 \tag{A6}$$

This represents a plane surface which intersects the U, V and W axes, respectively, at the points $(\frac{d^2}{2u_s}, 0, 0)$, $(0, \frac{d^2}{2v_s}, 0)$, and $(0, 0, \frac{d^2}{2w_s})$. It is simple to prove that the plane defined by equation (A6) perpendicularly bisects the line PS. The following corollary follows from Theorem A.

Corollary A

Let P and S be two fixed points in a two-dimensional UV–space and a distance d apart from one another, and let T be an arbitrary point in this space. If the ratio of the distances PT and ST is constant then the locus of points T defines

(a) a circle with centre located along the line PS, for a non-unity distance ratio.

(b) a straight line perpendicularly bisecting the line PS, for a unity distance ratio.

The proof of this corollary follows directly from the proof of Theorem A by eliminating the W–axis (equating the w–coordinates in equations (A1) - (A6) to zero).